Available online at www.sciencedirect.com
SCIENCE DIRECT®
Journal of Computational Physics 207 (2005) 639–659
JOURNAL OF COMPUTATIONAL PHYSICS
www.elsevier.com/locate/jcp

Boundary conditions for the upwind finite difference Lattice Boltzmann model: Evidence of slip velocity in micro-channel flow

Victor Sofonea [a,b,*], Robert F. Sekerka [b]

[a] *Laboratory for Numerical Simulation and Parallel Computing in Fluid Mechanics, Center for Fundamental and Advanced Technical Research, Romanian Academy, Bd. Mihai Viteazul 24, RO-300223 Timişoara, Romania*
[b] *Department of Physics, Carnegie Mellon University, 6416 Wean Hall, Pittsburgh, Pennsylvania 15213, USA*

Received 15 April 2004; received in revised form 1 November 2004; accepted 2 February 2005

Abstract

We conduct a systematic study of the effect of various boundary conditions (bounce back and three versions of diffuse reflection) for the two-dimensional first-order upwind finite difference Lattice Boltzmann model. Simulation of Couette flow in a micro-channel using the diffuse reflection boundary condition reveals the existence of a slip velocity that depends on the Knudsen number $\varepsilon = \lambda/L$, where λ is the mean free path and L is the channel width. For walls moving in opposite directions with speeds $\pm u_w$, the slip velocity satisfies $u_{\text{slip}} = 2\varepsilon u_{\text{wall}}/(1 + 2\varepsilon)$. In the case of Poiseuille flow in a micro-channel, the slip velocity is found to depend on the lattice spacing δs and Knudsen number ε to both first and second order. The best results are obtained for diffuse reflection boundary conditions that allow thermal mixing at a wall located at half lattice spacing outside the boundary nodes.

PACS: 03.40.Gc; 05.20.Dd; 47.11.+j

Keywords: Lattice Boltzmann; Boundary conditions; Slip velocity

* Corresponding author.
E-mail addresses: sofonea@acad-tim.tm.edu.ro (V. Sofonea), rs07@andrew.cmu.edu (R.F. Sekerka).

0021-9991/$ - see front matter © 2005 Elsevier Inc. All rights reserved.
doi:10.1016/j.jcp.2005.02.003

1. Introduction

Because of their intrinsic kinetic nature, Lattice Boltzmann (LB) models [1–4] are effective for problems where both mesoscopic dynamics and microscopic statistics become important, as in the case of micro-channel flows [5]. When the magnitude of the mean free path λ of fluid molecules becomes comparable to the channel width L (which means the Knudsen number $\varepsilon = \lambda/L$ exceeds 0.01), the slip velocity at the flow boundary (i.e., the channel walls) becomes noticeable. Since the continuum hypothesis is no longer valid when the Knudsen number becomes too large, the use of macroscopic equations such as the Navier–Stokes equation becomes questionable, even if associated with appropriate slip and temperature jump conditions at the wall surface [5]. For such problems, the use of LB models provides a promising alternative [6,7]; however, the results of computer simulations may be strongly affected by the boundary conditions imposed at the channel wall.

The purpose of the present paper is to investigate the influence of various procedures for handling boundary conditions in finite difference Lattice Boltzmann (FDLB) models on the apparent value of the slip velocity. FDLB models [8–13] are more general than standard LB models like the D2Q9 one [14] where the propagation speed depends on the mass of the fluid particles and also is related to the lattice spacing [15–17]. FDLB models allow to incorporate different propagation speeds on the same lattice, which is especially important in the case of multicomponent fluid system whose particles have different masses or in the case of multispeed thermal models [18].

We first give a general description of isothermal LB models in Section 2. For tractability in this paper we will restrict ourselves to the upwind finite difference LB model, which is introduced in Section 3; other FDLB models, like those discussed in [13], may be handled in a similar way. Although of first order, the upwind scheme is still preferable instead of higher order FDLB models (like the centered one, the Lax–Wendroff or the second-order upwind scheme) because of its simplicity and good numerical stability when large values of the density gradient are present in the fluid [19]. The upwind FDLB model will be used to simulate isothermal flow (Couette and Poiseuille) of a single component fluid in a 2D micro-channel, in the incompressible limit (i.e., low Mach number). The appropriate boundary conditions for the distribution functions are introduced in Section 4 while the problem of the slip velocity in channel flow is briefly discussed in Section 5. Simulation results, as well as the effect of the lattice spacing and the Knudsen number on the slip velocity, are discussed further in Section 6.

2. General description of LB models

Finite difference Lattice Boltzmann models [13,8–12] are derived from the continuous Boltzmann equation with the collision term in the Bhatnagar–Gross–Krook (BGK) approximation [20,21]

$$\left(\frac{\partial}{\partial t} + \mathbf{v}\cdot\nabla + \frac{\mathbf{F}}{m}\cdot\nabla_{\mathbf{v}}\right) f(\mathbf{x},\mathbf{v},t) = -\frac{1}{\tau}\left[f(\mathbf{x},\mathbf{v},t) - f^{\mathrm{eq}}(\mathbf{x},\mathbf{v},t)\right], \tag{1}$$

where τ is the relaxation time and $\mathbf{F} = m\mathbf{a}$ is the external force acting on a fluid particle whose mass is m. In a D-dimensional space, the equilibrium distribution function of an ideal gas is the well-known Maxwell–Boltzmann distribution

$$f^{\mathrm{eq}}(\mathbf{x},\mathbf{v},t) = n(\mathbf{x},t)\left(\frac{m}{2\pi k_{\mathrm{B}}T}\right)^{D/2} \mathrm{e}^{-\frac{m}{2k_{\mathrm{B}}T}[\mathbf{v}-\mathbf{u}(\mathbf{x},t)]^2}, \tag{2}$$

where

$$n \equiv n(\mathbf{x},t) = \int f^{\mathrm{eq}}(\mathbf{x},\mathbf{v},t)\mathrm{d}^D v \tag{3}$$

is the local number density and

$$\mathbf{u} \equiv \mathbf{u}(\mathbf{x},t) = \frac{1}{n(\mathbf{x},t)} \int \mathbf{v} f^{\mathrm{eq}}(\mathbf{x},\mathbf{v},t)\mathrm{d}^D v \tag{4}$$

is the local velocity.

For a system not too far from its equilibrium state, we may suppose

$$\nabla_{\mathbf{v}} f(\mathbf{x},\mathbf{v},t) \simeq \nabla_{\mathbf{v}} f^{\mathrm{eq}}(\mathbf{x},\mathbf{v},t) = -\frac{m}{k_{\mathrm{B}}T}[\mathbf{v}-\mathbf{u}(\mathbf{x},t)]f^{\mathrm{eq}}(\mathbf{x},\mathbf{v},t). \tag{5}$$

After introducing expression (5) in Eq. (1), we get the following form of the Boltzmann equation:

$$\partial_t f(\mathbf{x},\mathbf{v},t) + \mathbf{v}\cdot\nabla f(\mathbf{x},\mathbf{v},t) = \frac{1}{k_{\mathrm{B}}T}\mathbf{F}\cdot[\mathbf{v}-\mathbf{u}(\mathbf{x},t)]f^{\mathrm{eq}}(\mathbf{x},\mathbf{v},t) - \frac{1}{\tau}[f(\mathbf{x},\mathbf{v},t) - f^{\mathrm{eq}}(\mathbf{x},\mathbf{v},t)], \tag{6}$$

which provides the starting point for any FDLB model.

The central idea of Lattice Boltzmann models is the discretization of velocity space [1–4,15,16]. The velocity space is restricted to a finite set $\{\mathbf{e}_i\}$, $i = 0,1,\ldots,\mathscr{N}$ with new distribution functions $f_i(\mathbf{x},t)$ that replace $f(\mathbf{r},\mathbf{v},t)\mathrm{d}^D v$ for $\mathbf{v} = \mathbf{e}_i$. To solve the resulting equations, one usually discretizes the physical space and uses nodes $\mathbf{x}$ of a lattice $\mathscr{L}$. After discretization of both $\mathbf{v}$ and $\mathbf{x}$, the BGK Boltzmann equation (6) becomes a system of $\mathscr{N}$ equations

$$\partial_t f_i(\mathbf{x},t) + \mathbf{e}_i\cdot\nabla f_i(\mathbf{x},t) = \frac{1}{k_{\mathrm{B}}T}\mathbf{F}\cdot[\mathbf{e}_i-\mathbf{u}(\mathbf{x},t)]f_i^{\mathrm{eq}}(\mathbf{x},t) - \frac{1}{\tau}[f_i(\mathbf{x},t) - f_i^{\mathrm{eq}}(\mathbf{x},t)] \quad (i = 0,1,\ldots\mathscr{N}). \tag{7}$$

The distribution function $f_i(\mathbf{x},t)$ is the probability of finding at node $\mathbf{x} \in \mathscr{L}$ a particle of mass m having the velocity $\mathbf{e}_i$. When using a two-dimensional (2D) square lattice (like the one shown in Fig. 1, which refers to the so-called D2Q9 model [14]), $\mathscr{N} = 8$ and the velocities $\mathbf{e}_i$ are given by

$$\mathbf{e}_i = \begin{cases} 0 & (i=0), \\ \left[\cos\frac{(i-1)\pi}{2}, \sin\frac{(i-1)\pi}{2}\right]c & (i=1,\ldots,4), \\ \left[\cos\left(\frac{\pi}{4}+\frac{(i-5)\pi}{2}\right), \sin\left(\frac{\pi}{4}+\frac{(i-5)\pi}{2}\right)\right]\sqrt{2}c & (i=5,\ldots,8). \end{cases} \tag{8}$$

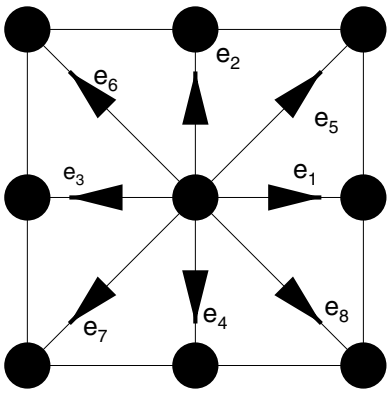

Fig. 1. Velocities in the D2Q9 Lattice Boltzmann model.

Here, c is the propagation speed of particles moving between a lattice node and its nearest neighbors. Following the procedure introduced in [15–17], this velocity is related to the thermal velocity of the fluid particles and is determined by the fluid temperature T, the Boltzmann constant k_B, as well as the mass m of these particles:

$$c = \sqrt{\frac{k_B T}{\chi m}}. \tag{9}$$

The value of the constant χ is a characteristics of the LB model. For the D2Q9 model [14] used in this paper, we have $\chi = 1/3$ [17].

The equilibrium distribution functions in (7) are given as series expansions in the local velocity $\mathbf{u} = \mathbf{u}(\mathbf{x}, t)$ [17,22],

$$f_i^{\mathrm{eq}} = f_i^{eq}(\mathbf{x}, t) = w_i n \left[1 + \frac{\mathbf{e}_i \cdot \mathbf{u}}{\chi c^2} + \frac{(\mathbf{e}_i \cdot \mathbf{u})^2}{2\chi^2 c^4} - \frac{\mathbf{u} \cdot \mathbf{u}}{2\chi c^2}\right] \quad (i = 0, 1, \ldots, 8), \tag{10}$$

where the weight factors w_i are

$$w_i = \begin{cases} \frac{4}{9} & (i = 0), \\ \frac{1}{9} & (i = 1, \ldots, 4), \\ \frac{1}{36} & (i = 5, \ldots, 8). \end{cases} \tag{11}$$

If we use the series expansion (10) in the expression of the force term which appears in the evolution Eq. (7) and restrict the result up to first-order terms in the local velocity $\mathbf{u}$, we get

$$\frac{1}{k_B T}\mathbf{F} \cdot [\mathbf{e}_i - \mathbf{u}] f_i^{\mathrm{eq}} = \frac{w_i n}{m}\mathbf{F} \cdot \left[\frac{\mathbf{e}_i - \mathbf{u}}{\chi c^2} + \frac{(\mathbf{e}_i \cdot \mathbf{u})\mathbf{e}_i}{\chi c^4}\right], \tag{12}$$

which is equivalent to the expression already derived in [17,23].

As a result of the discretization of phase space, integrals in this space are replaced by sums over the discrete velocity set $\{\mathbf{e}_i\}$. Consequently, expression (3) of the local number density becomes

$$n \equiv n(\mathbf{x}, t) = \sum_{i=0}^{N} f_i(\mathbf{x}, t), \tag{13}$$

while the local velocity (4) is replaced by

$$\mathbf{u} \equiv \mathbf{u}(\mathbf{x}, t) = \frac{1}{n(\mathbf{x}, t)} \sum_{i=0}^{N} \mathbf{e}_i f_i(\mathbf{x}, t). \tag{14}$$

Two techniques may be used to derive the fluid equations from the Boltzmann equation (7): Grad's method of moments [24–26] or the Chapman–Enskog expansion [1–4,22]. When using the latter approach, the distribution functions are formally expanded as series in the Knudsen number $\varepsilon = c\tau/L$, where L is the system size

$$f_i = \sum_{l=0}^{\infty} \varepsilon^l f_i^{(l)} = f_i^{(0)} + \varepsilon f_i^{(1)} + \varepsilon^2 f_i^{(2)} + \cdots \tag{15}$$

Two time scales and one length scale are also adopted

$$t = \varepsilon^{-1} t_1 + \varepsilon^{-2} t_2, \tag{16}$$

$$\mathbf{r} = \varepsilon^{-1}\mathbf{r}_1, \tag{17}$$

such that the time and space derivatives are expressed as

$$\partial_t = \varepsilon\partial_{t_1} + \varepsilon^2\partial_{t_2}, \tag{18}$$

$$\nabla_{\mathbf{r}} = \varepsilon\nabla_{\mathbf{r}_1}. \tag{19}$$

These expressions are substituted into Eq. (7) and terms involving ε to zero-th, first and second order are separated. After some algebra, the mass and momentum conservation equations are derived up to second order in the Knudsen number

$$\partial_t\rho + \partial_\beta(\rho u_\beta) = 0, \tag{20}$$

$$\partial_t(\rho u_\alpha) + \partial_\beta(\rho u_\alpha u_\beta) = -\partial_\alpha p + \nu\partial_\beta\left[\rho\partial_\alpha u_\beta + \rho\partial_\beta u_\alpha\right] + \rho a_\alpha, \tag{21}$$

where

$$p := nk_{\mathrm{B}}T = \chi c^2\rho \tag{22}$$

is the ideal gas pressure ($\rho = mn$). The Navier–Stokes equation is recovered from (21) in the incompressible limit ($\partial_\beta u_\beta = 0$)

$$\partial_t u_\alpha + u_\beta\partial_\beta u_\alpha = -\frac{1}{\rho}\partial_\alpha p + \nu\nabla^2 u_\alpha + a_\alpha. \tag{23}$$

Here, ν is the *physical value* of the kinematic viscosity of the single component fluid

$$\nu = \tau\chi c^2 = \tau k_{\mathrm{B}}T/m. \tag{24}$$

The above expression of the kinematic viscosity, which can also be derived by using the method of moments [25,26], is of principal importance since it expresses the fact that the behavior of the fluid we simulate with the LB model is independent of the discretization of the phase space (i.e., independent of $\mathscr{N}$ or χ). However, the numerical scheme used to solve the spatial and temporal aspect of the LB model may introduce a numerical viscosity that adds to the *physical value* (24) to give an *apparent value* of the kinematic viscosity, as discussed in [13].

3. The upwind finite difference Lattice Boltzmann model

The set of phase space discretized Boltzmann equations (7) for the distribution functions $f_i \equiv f_i(\mathbf{x}, t)$ may be solved numerically by using an appropriate finite difference scheme defined on the lattice $\mathscr{L}$ [13]. When using a scheme based on characteristics, the forward Euler difference is used to compute the time derivative, but there are several possibilities [27,28] to compute the term $\mathbf{e}_i \cdot \nabla f_i(\mathbf{x}, t)$. We will restrict here to the *first-order upwind scheme*; other finite difference schemes for LB models are discussed in [13]. Following this scheme, the distribution functions are updated at each lattice node in accordance to

$$\begin{aligned} f_i(\mathbf{x}, t+\delta t) = f_i(\mathbf{x}, t) &- \frac{c\delta t}{\delta s}\left[f_i(\mathbf{x}, t) - f_i(\mathbf{x} - \delta s\mathbf{e}_i/c, t)\right] - \frac{\delta t}{\tau}\left[f_i(\mathbf{x}, t) - f_i^{\mathrm{eq}}(\mathbf{x}, t)\right] \\ &+ \frac{\delta t}{\chi c^2}\mathbf{a}(\mathbf{x}, t)\cdot\left[\mathbf{e}_i - \mathbf{u}(\mathbf{x}, t)\right]f_i^{\mathrm{eq}}(\mathbf{x}, t) \quad (i = 0, 1, \ldots \mathscr{N}), \end{aligned} \tag{25}$$

where δs is the lattice spacing and δt is the time step.

As discussed in [13], the correct mass equation (20) is recovered in the incompressible limit (constant ρ and small Mach number). The apparent value of the kinematic viscosity, which enters the Navier–Stokes equation (23) when using the first-order upwind scheme is [13]

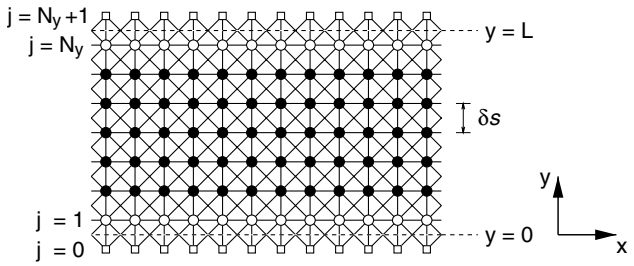

Fig. 2. The square lattice used for finite difference LB simulation of channel flow (●, bulk nodes; ○, boundary nodes; □, ghost nodes outside the walls). Walls are situated along the dashed lines (at half lattice spacing between boundary nodes and ghost nodes). Periodic boundary conditions are used in the horizontal direction.

$$v = \chi c^2 \left[\tau + \frac{\delta s}{2c}\right]. \tag{26}$$

Fig. 2 shows the square lattice used to simulate isothermal channel flow in 2D. Application of the updating rule (25) in the *bulk nodes* is straightforward. The same holds for lattice nodes where periodic boundary conditions in the x direction apply. Special attention should be paid when applying the updating rule (25) to the *boundary nodes* (i.e., those fluid nodes located near the channel wall, which have $j = 1$ or $j = N_y$) since the distribution functions $f_i(\mathbf{x} - \delta s\mathbf{e}_i/c, t)$ are not defined for certain values of the index i. The *ghost nodes* where the distribution functions $f_i(\mathbf{x} - \delta s\mathbf{e}_i/c, t)$ should be evaluated (i.e., the lattice nodes with $j = 0$ or $j = N_y + 1$) are outside the fluid domain and we must provide appropriate handling rules. Although this paper refers only to the upwind finite difference scheme, the rules discussed in the next section provide the boundary conditions for a larger class of characteristics based finite difference LB models where a single row of ghost nodes should be considered outside the walls; this class includes other schemes already discussed in [13]: the Lax–Friedrichs scheme, the Lax–Wendroff scheme, as well as the space centered scheme.

4. Boundary conditions

4.1. Physical considerations

In this paper, we will restrict ourselves to boundary conditions for 2D channel flow. We use an $N_x \times (N_y + 2)$ square lattice with periodic boundary conditions in the horizontal (x) direction (Fig. 2), with the walls placed at half lattice spacing outside boundary nodes. When using non-dimensional equations, the channel width is $L = 1$ and the lattice spacing is $\delta s = 1/N_y$. Walls may be at rest or may move along the horizontal axis x.

Gas particles may strike and reflect from walls. When a wall is at rest, the so called *bounce back* case is usually considered in LB models, as well as in Lattice Gas simulations [1–4]. In this case, incident particles are reflected by the wall in the opposite direction (Fig. 3(a)). However, there are other possibilities. If gas particles collide with an idealized wall that is perfectly smooth on the molecular scale, no shear forces will be transmitted and their tangential momentum will be conserved. In this case, as illustrated in Fig. 3(b), the angle of incidence is equal to the angle of reflection. This is called *specular reflection* and there is perfect slip at the wall. For the opposite case, when walls are considered to be extremely rough at the molecular scale, gas particles are assumed to reflect at some random angle that is uncorrelated with their angle of incidence. In this *diffuse reflection* case (Fig. 3(c)), the velocities of particles leav-

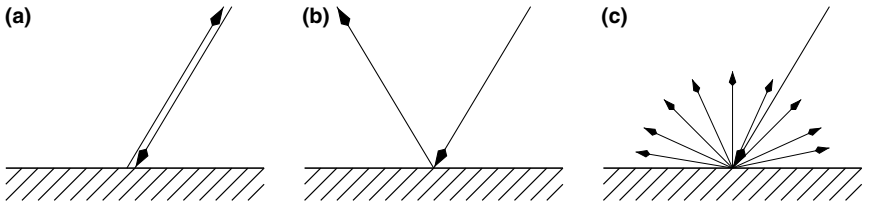

Fig. 3. Boundary conditions for the distribution functions: (a) Bounce back; (b) specular reflection; (c) diffuse reflection.

ing the wall are assumed to follow the Maxwellian distribution law [29–32]. The parameters that define the Maxwellian distribution of the diffuse reflected gas particles are the wall velocity $\mathbf{u}_{\text{wall}}$ and the wall temperature T_{wall}. In this paper, we deal only with isothermal systems so the wall temperature is assumed to equal the fluid temperature T. For real walls, some gas molecules reflect diffusively while other molecules reflect specularly; this more general case may be considered by introducing an accomodation coefficient [5,31–33] but we shall not discuss this case here.

4.2. Implementation of boundary conditions for the distribution functions

If the node $\mathbf{x}$ is a boundary node (i.e., a node located on the first row near the bottom wall of the channel, like the central node in Fig. 4, whose indices are k,j, with $j = 1$), the updating rule (25) cannot be used for all distribution functions $f_i(\mathbf{x},t) \equiv f_i^{k,j=1}$ $(i = 0,1,\ldots,\mathcal{N})$ since some of the values of the distribution functions $f_i^{k,j=0}$ are undefined. For the node $(k,j = 1)$ in Fig. 4, the missing values refer to $i \in \{2,5,6\}$. For convenience, we will refer further to this case since the case of a node located near the top wall may be handled in a similar way.

The missing values of the distribution functions defined in ghost nodes ($j = 0$) may be estimated using one of the following procedures for the *boundary conditions*:

(a) *Bounce back*

Particles originating from the node $k,1$ are bounced back in the points marked L, M, R on the wall. Consequently, we have

$$\begin{aligned} f_2^{k,0} &= f_4^{k,1}, \\ f_5^{k-1,0} &= f_7^{k,1}, \\ f_6^{k+1,0} &= f_8^{k,1} \end{aligned} \tag{27}$$

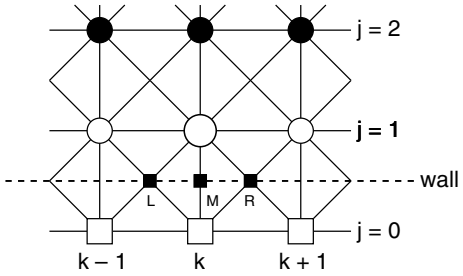

Fig. 4. Boundary nodes ($j = 1$) and ghost nodes ($j = 0$) at the bottom wall. Particles originating from the node $(k,j = 1)$ are reflected in the points marked L, M, R on the wall.

(b) *Specular reflection*

In this case, particles originated from boundary nodes (with $j = 1$) are reflected specularly in the wall points L, M, R, such that

$$\begin{aligned} f_2^{k,0} &= f_4^{k,1}, \\ f_5^{k-1,0} &= f_8^{k-1,1}, \\ f_6^{k+1,0} &= f_7^{k+1,1}. \end{aligned} \tag{28}$$

(c) *Diffuse reflection (version 1)*

To get particles reflected diffusely at time t in the wall node point L (Fig. 4), we first note that this point receives particles originating from lattice boundary nodes $(k-1,1)$ and $(k,1)$. The distribution functions of these particles mix together and redirect thereafter towards the same nodes because the discrete character of the velocity space in LB simulations does not allow other possible directions. If we denote by f_5^{L} and also f_6^{L} the LB distribution functions of the particles at the wall point L which, after diffuse reflection, have the velocities $\mathbf{e}_5$ and $\mathbf{e}_6$, respectively, we may compute these distribution functions by linear interpolation of the distribution functions defined in the boundary nodes ($j = 1$), as well in the ghost nodes ($j = 0$):

$$\begin{aligned} f_5^{\mathrm{L}} &= \frac{f_5^{k-1,0} + f_5^{k,1}}{2}, \\ f_6^{\mathrm{L}} &= \frac{f_6^{k-1,1} + f_6^{k,0}}{2}. \end{aligned} \tag{29}$$

In the updating rule (25), information on the particles diffusively reflected from the point L towards node $(k,1)$ is contained in the value of $f_5^{k-1,0}$, while the information on the particles redirected towards node $(k-1,1)$ is contained in $f_6^{k,0}$. Because of the mixing process that takes place at the point L of the wall, the diffusely reflected distribution functions f_5^{L} and f_6^{L} (or, equivalently, the unknown quantities $f_5^{k-1,0}$ and $f_6^{k,0}$) should be dependent on both incoming distribution functions $f_7^{k,1}$ and $f_8^{k-1,1}$. Conservation of particle number diffusely reflected in point L requires

$$f_5^{k-1,0} + f_6^{k,0} = f_7^{k,1} + f_8^{k-1,1}. \tag{30}$$

A second equation to be fulfilled by $f_5^{k-1,0}$ and $f_6^{k,0}$ may be derived from the requirement that the diffusely reflected distribution functions f_5^{L} and f_6^{L} defined in at the wall point L follow the Maxwellian distribution whose mean velocity is the bottom wall velocity $\mathbf{u}_{\mathrm{bot\_wall}}$. Thus $f_5^{\mathrm{L}}/f_5^{\mathrm{eq}} = f_6^{\mathrm{L}}/f_6^{\mathrm{eq}}$ for $\mathbf{u} = \mathbf{u}_{\mathrm{bot\_wall}}$. In view of Eqs. (10) and (29) we obtain

$$\frac{f_5^{k-1,0} + f_5^{k,1}}{s_5} = \frac{f_6^{k-1,1} + f_6^{k,0}}{s_6}, \tag{31}$$

where

$$s_i = w_i \left[1 + \frac{\mathbf{e}_i \cdot \mathbf{u}_{\mathrm{bot\_wall}}}{\chi c^2} + \frac{\left(\mathbf{e}_i \cdot \mathbf{u}_{\mathrm{bot\_wall}}\right)^2}{2\chi^2 c^4} - \frac{\mathbf{u}_{\mathrm{bot\_wall}} \cdot \mathbf{u}_{\mathrm{bot\_wall}}}{2\chi c^2} \right]. \tag{32}$$

By solving Eqs. (30) and (31), we can get values of $f_5^{k-1,0}$ and $f_6^{k,0}$. A similar procedure applied to the wall point R gives values of $f_5^{k,0}$ and $f_6^{k+1,0}$. The value of $f_2^{k,0}$ may be derived from the bounce back scheme since no particle mixing occurs at the wall node M in Fig. 4. The final results for the three ghost points needed to update $f_i^{k,j=1}$ are

$$
\begin{aligned}
f_2^{k,0} &= f_4^{k,1},\\
f_5^{k-1,0} &= \frac{s_5\left(f_6^{k-1,1}+f_7^{k,1}+f_8^{k-1,1}\right)-s_6 f_5^{k,1}}{s_5+s_6},\\
f_6^{k+1,0} &= \frac{s_6\left(f_5^{k+1,1}+f_7^{k+1,1}+f_8^{k,1}\right)-s_5 f_6^{k,1}}{s_5+s_6}.
\end{aligned}
\tag{33}
$$

(d) *Diffuse reflection (version 2)*

We can consider that the mixing process takes place in the ghost nodes instead of the wall points L and R. The ghost node $(k,j=0)$ receives particles coming from nodes $(k-1,j=1)$, $(k,j=1)$ and $(k+1,j=1)$. The distribution functions of incoming particles are $f_8^{k-1,1}, f_4^{k,1}$ and $f_7^{k+1,1}$, respectively. Preservation of the total number of particles requires the number of outcoming particles to equal the number of incoming particles in ghost nodes

$$
f_8^{k-1,1}+f_4^{k,1}+f_7^{k+1,1}=f_5^{k,0}+f_2^{k,0}+f_6^{k,0}=n_{(2)}^k. \tag{34}
$$

According to physical considerations concerning diffuse reflection, we use the fact that the distribution functions of outcoming particles are Maxwellian. This allows us to compute the values of these functions in the ghost nodes

$$
f_i^{k,0}=s_i n_{(2)}^k \quad (i=2,5,6), \tag{35}
$$

where coefficients s_i are given by Eq. (32).

(e) *Diffuse reflection (version 3)*

In this version of the diffuse reflection rule, the value of the distribution function $f_2^{k,0}$ is derived using the bounce back rule, while the values of the two remaining distribution functions to be computed in the ghost node $(k,j=0)$ are derived using a mixing procedure similar to version 2:

$$
f_2^{k,0}=f_4^{k,1}, \tag{36}
$$

$$
f_i^{k,0}=s_i n_{(3)}^k \quad (i=5,6), \tag{37}
$$

where coefficients s_i are given again by Eq. (32) and

$$
n_{(3)}^k=f_8^{k-1,1}+f_7^{k+1,1}=f_5^{k,0}+f_6^{k,0}. \tag{38}
$$

All five procedures (a)–(e) introduced above preserve the total number of fluid particles in the lattice $\mathscr{L}$:

$$
N_{total}(t)=\sum_{\mathbf{x}\in\mathscr{L}}\sum_{i=0}^{i=8} f_i(\mathbf{x},t)=\text{constant}. \tag{39}
$$

This may be checked after summation of the finite difference LB equation (25) and use of the general properties of the distribution functions $f_i^{\sigma}, f_i^{\sigma,\mathrm{eq}}$, as well as the corresponding expressions of the values of the distribution functions in the ghost nodes.

5. Slip velocity

The problem of boundary conditions for channel flow is still an open one, especially for the case of multicomponent fluids [34–36] because of physical interactions which may occur between fluid particles and wall particles. Although it is widely accepted that the normal component of the fluid velocity should vanish at the walls, there are two extreme cases concerning the tangential component of the fluid velocity with

respect to the wall: the so called *free slip* and the *no-slip* boundary conditions [5]. In the first case, the fluid velocity relative to the wall may have a non-zero tangential component, while this component vanishes in the second case, as the normal component always does.

The kinetic theory of gases [5,29,32,37,38] relates the tangential velocity slip at the wall $u_{\text{slip}} \equiv \Delta u|_{\text{wall}}$ to the local shear through a series expansion in the mean free path λ, or, equivalently, in the Knudsen number $\varepsilon = \lambda/L$, where L is the reference length (i.e., the channel width). The general second-order slip condition is [5]

$$u_{\text{slip}} \equiv \Delta u|_{\text{wall}} = u_{fluid}|_{\text{wall}} - u_{\text{wall}} = C_1 \varepsilon \left.\frac{\partial u}{\partial \eta}\right|_{\text{wall}} - C_2 \varepsilon^2 \left.\frac{\partial^2 u}{\partial \eta^2}\right|_{\text{wall}} \tag{40}$$

where $u_{\text{fluid}}|_{\text{wall}}$ is the tangential component of the fluid velocity on the wall, u_{wall} is the wall velocity (as mentioned in Section 4.1, walls may be at rest or may move along themselves, i.e., along the x axis in Fig. 2) and η is the distance from the wall, measured in units of L, whose positive direction points towards the fluid. The values of the coefficients C_1 and C_2 in the above expression of the slip velocity are dependent on the kinetic models developed by various investigators [5,29,32]. The value $C_1 = 1$ is a characteristic of most models, including a first-order model already derived by Maxwell in 1879 [39], but the value of the coefficient C_2 is still disputed in the literature [5]. We will determine the values of the coefficients C_1 and C_2 from the results of our FDLB simulations.

In accordance to Eq. (40), there is always a velocity slip at the wall when $\partial u/\partial \eta|_{\text{wall}} \neq 0$, but this slip velocity is negligible for small values of the Knudsen number ε. The slip velocity becomes important only when the Knudsen number exceeds the value $\varepsilon = 0.01$ and the continuum hypothesis breaks down [5]. This happens in thin channels (micro-channels), whose characteristic length (width or thickness) is comparable to the mean free path of fluid particles. However, in the so-called *slip flow* domain ($0.1 \geqslant \varepsilon \geqslant 0.01$), it is widely recognized that the well-known Navier–Stokes equations of the continuum media mechanics may be still used provided the no-slip hypothesis is rejected and the existence of the slip velocity is entered into the boundary conditions [5,32]. To clarify this subject, we will consider here two well-known cases of stationary flow in micro-channels:

(a) *Couette flow*

Couette flow results from the steady, relative motion of the two walls in Fig. 2. As walls move along the horizontal (x) axis, the fluid is set into motion because of the interaction with the walls. We consider the case for which the bottom wall moves with the velocity $\mathbf{u}_{\text{wall\_bot}} = (-u_w, 0)$ while the top wall moves with the velocity $\mathbf{u}_{\text{wall\_top}} = (u_w, 0)$, and search for a stationary solution of the form

$$u_x = u_x(y), \quad u_y = 0 \quad (0 \leqslant y/L \leqslant 1). \tag{41}$$

For this case, the incompressible Navier–Stokes equation (23) becomes, with p = constant and $\mathbf{a} = 0$:

$$\nabla^2 \mathbf{u} = 0. \tag{42}$$

The general form of the x component of the fluid velocity (41) is thus a linear function of the y coordinate:

$$u_x(y) = A(y/L) + B. \tag{43}$$

The coefficients A and B of this solution may be found using the boundary condition (40):

$$\begin{aligned} u_x(0) &= -u_w + u_{\text{slip}} = -u_w + C_1 \varepsilon A = B, \\ u_x(L) &= u_w + u_{\text{slip}} = u_w - C_1 \varepsilon A = A + B. \end{aligned} \tag{44}$$

Thus, Eq. (43) becomes

$$u_x(y) = \frac{u_w}{1 + 2C_1 \varepsilon}(2y/L - 1), \tag{45}$$

and the magnitude of the fluid velocity at the walls

$$|u_x(0)| = |u_x(L)| = \frac{u_w}{1 + 2C_1\varepsilon} \tag{46}$$

equals the wall velocity only in the limit case $\varepsilon \to 0$. In the opposite limit case ($\varepsilon \to \infty$), the fluid remains at rest.

(b) *Poiseuille flow*

In this case, the walls are at rest ($u_w = 0$), but the fluid moves under the action of an external force parallel to the walls. We will consider again the incompressible Navier–Stokes equation (23) with p = constant and $a_x = a$, $a_y = 0$. When searching for a stationary solution of the form (41), (23) reduces to

$$v\nabla^2 u_x + a = 0, \tag{47}$$

and we get the general solution

$$u_x(y) = A(y/L)^2 + B(y/L) + C \tag{48}$$

with

$$A = -\frac{aL^2}{2v}. \tag{49}$$

The remaining coefficients B and C are found from the boundary condition (40):

$$\begin{aligned} u_x(0) &= C_1\varepsilon B - 2C_2\varepsilon^2 A, \\ u_x(L) &= -C_1\varepsilon(2A + B) - 2C_2\varepsilon^2 A. \end{aligned} \tag{50}$$

This gives the final form of the stationary solution

$$u_x(y) = \frac{aL^2}{2v}[-(y/L)^2 + (y/L) + C_1\varepsilon + 2C_2\varepsilon^2], \tag{51}$$

while the fluid (slip) velocity at the wall is

$$u_x(0) = u_x(L) = \frac{aL^2}{2v}[C_1\varepsilon + 2C_2\varepsilon^2]. \tag{52}$$

If we compute the mean value of the fluid velocity in the channel

$$\bar{u} = \frac{1}{L}\int_0^L u_x(y)\mathrm{d}y = \frac{aL^2}{2v}\left[\frac{1}{6} + C_1\varepsilon + 2C_2\varepsilon^2\right], \tag{53}$$

the following characteristics of the velocity profile may be derived:

$$\frac{u_{max}}{\bar{u}} = \frac{u_x(L/2)}{\bar{u}} = \frac{1/4 + C_1\varepsilon + 2C_2\varepsilon^2}{1/6 + C_1\varepsilon + 2C_2\varepsilon^2}, \tag{54}$$

$$\frac{u_{\mathrm{slip}}}{\bar{u}} = \frac{u_x(0)}{\bar{u}} = \frac{u_x(L)}{\bar{u}} = \frac{C_1\varepsilon + 2C_2\varepsilon^2}{1/6 + C_1\varepsilon + 2C_2\varepsilon^2}. \tag{55}$$

For $\varepsilon \to 0$, we get

$$\begin{aligned} \frac{u_{\max}}{\bar{u}} &= 1.5, \\ \frac{u_{\mathrm{slip}}}{\bar{u}} &= 0, \end{aligned} \tag{56}$$

while for $\varepsilon \to \infty$, we get

$$\frac{u_{\max}}{\bar{u}} = \frac{u_{\text{slip}}}{\bar{u}} = 1. \tag{57}$$

In order to compare with computer simulation results, we rewrite Eq. (26) in the form

$$v = \chi c L\left[\varepsilon + \frac{\delta s}{2L}\right] = \chi c L\left[\varepsilon + \frac{1}{2N_y}\right], \tag{58}$$

where N_y is the number of lattice nodes along the characteristic length L. Eq. (51) becomes

$$u_x(y) = u_\varepsilon\left[-(y/L)^2 + (y/L) + C_1\varepsilon + 2C_2\varepsilon^2\right], \tag{59}$$

where

$$u_\varepsilon = \frac{u_a}{\varepsilon + \frac{1}{2N_y}} \tag{60}$$

and

$$u_a = \frac{aL}{2\chi c}. \tag{61}$$

The reference quantities u_ε and u_a introduced above will be used in the next section to get non-dimensional velocity profiles for Poiseuille flow.

6. Simulation results

6.1. Couette flow

For the simulation of Couette flow, we used the upwind finite difference LB model where the boundary conditions are expressed using the three versions of the *diffuse reflection* technique. The bounce back technique is not appropriate for this case since that technique may be applied only when the walls are at rest. All simulations were done with the same values of the wall velocity ($u_w = 0.001$) and time step ($\delta t = 0.001$).

Fig. 5 shows the stationary velocity profiles we get after 100,000 time steps using the first version of the diffuse reflection boundary condition, for $N_y = 100$ and various values of the Knudsen number $\varepsilon = c\tau/L$ (we remember that $c = 1$ and $L = 1$ when using the non-dimensional form of LB and fluid equations). We see that the slip velocity is negligible for $\varepsilon \leqslant 0.01$, since the value of the fluid velocity at the wall is practically equal to the wall velocity u_w. The increase of the slip velocity is noticeable when the Knudsen number becomes larger than 0.01, as expected in accordance to kinetic theories [5,29]. The stationary velocity profiles for Couette flow were found to be well superposed when using various values of the lattice spacing $\delta s = L/N_y$ (i.e., various number of lattice nodes in the y direction across the channel), regardless the value of the Knudsen number. To check the validity of Eq. (46) in the case of LB simulations done with the first version of the diffuse reflection boundary condition, we plot in Fig. 6 the quantity $u_w/u(L)$ against the Knudsen number ε. The agreement between our LB simulation results and Eq. (46) with $C_1 = 1$ is excellent. Further simulations (not shown here) revealed that the linear dependence of $u_w/u(L)$ with respect to the Knudsen number ε, which is predicted by Eq. (46), appears to be preserved in our model even for very large values of ε. However, the validity of the model for such large values of ε is uncertain and the number of time steps necessary to get the stationary state increases dramatically with the value of ε.

LB simulation results (velocity profiles) obtained with versions 2 and 3 of the diffuse reflection boundary condition were virtually indistinguishable. However, although linear, these profiles exhibit a noticeable

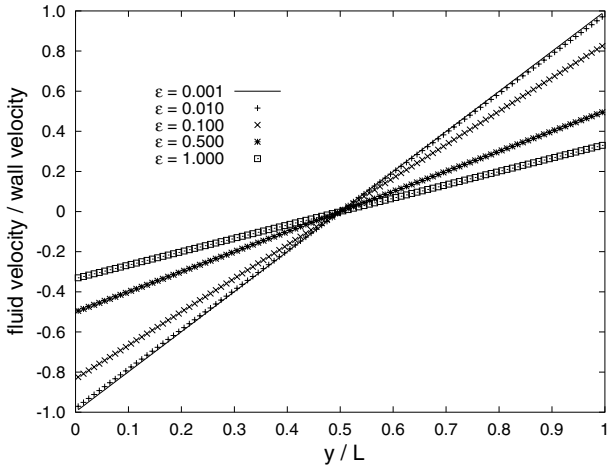

Fig. 5. Stationary velocity profiles of Couette flow for $N_y = 100$ ($\delta s/L = 0.01$) and various values of the Knudsen number (diffuse reflection boundary condition, version 1).

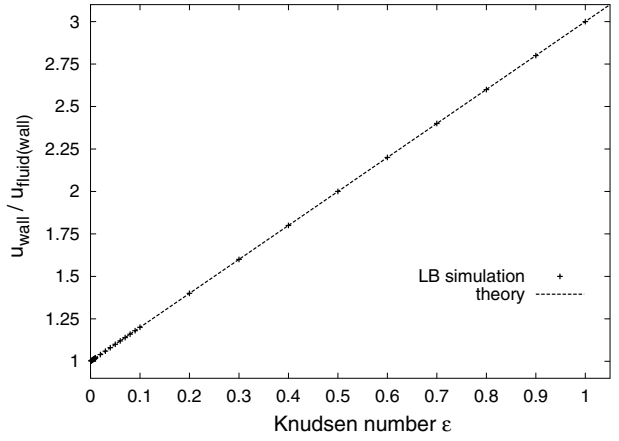

Fig. 6. Dependence of $u_w/u_x(L)$ vs. Knudsen number (diffuse reflection boundary conditions, version 1). The theoretical line is given by Eq. (46) with $C_1 = 1$.

dependence on the lattice spacing δs, as shown in Fig. 7 for $\varepsilon = 0.1$. To explain the effect of the lattice spacing on the slope of these velocity profiles, we recall that in version 2 and 3 of the diffuse reflection boundary condition, the wall velocity is actually imposed in the ghost nodes and not on the wall, as done in the first version. Thus, if we search for the values of the coefficients A and B in Eq. (43), we really have a slightly modified version of Eqs. (44):

$$\begin{aligned} u_x(-\delta s/2) &= -u_w + u_{\text{slip}} = -u_w + C_1 \varepsilon A = -A\delta s/2L + B, \\ u_x(L + \delta s/2) &= u_w + u_{\text{slip}} = u_w - C_1 \varepsilon A = A(1 + \delta s/2L) + B, \end{aligned} \tag{62}$$

which gives

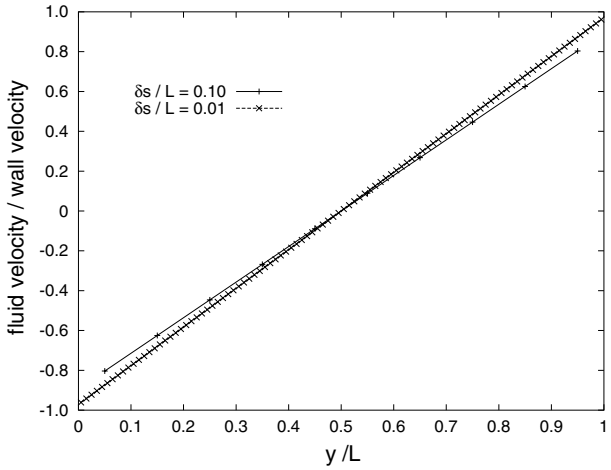

Fig. 7. Effect of the lattice spacing δs on the stationary velocity profiles of Couette flow for $\varepsilon = 0.1$ (diffuse reflection boundary condition, versions 2 and 3).

$$A = \frac{2u_w}{1 + \delta s/L + 2C_1\varepsilon}, \quad B = -\frac{u_w}{1 + \delta s/L + 2C_1\varepsilon}. \tag{63}$$

The above expression of the A coefficient is validated by our LB simulations in Fig. 8 where the dependence of the ratio $2u_w/A$ against the non-dimensional lattice spacing $\delta s/L$ is displayed for three values of the Knudsen number. For convenience, in Fig. 8 we checked also Eq. (46) which is valid for the first version of the diffuse reflection boundary condition, and we found no effect of the lattice spacing in this case.

6.2. Poiseuille flow

Fig. 9 shows the non-dimensional velocity profile $u(y/L)/u_a$ for Poiseuille flow for various values of the relaxation time τ, i.e., various values of the Knudsen number $\varepsilon = c\tau/L$ when version 1 of the diffuse reflec-

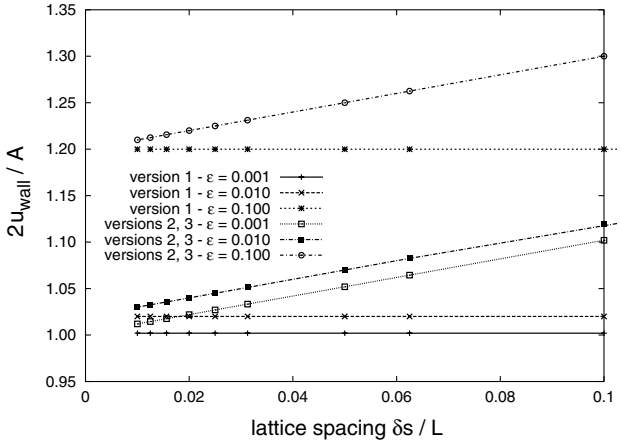

Fig. 8. Effect of the lattice spacing δs on the ratio $2u_{\text{wall}}/A$ (Couette flow) for three values of the Knudsen number and three versions of the diffuse reflection boundary conditions.

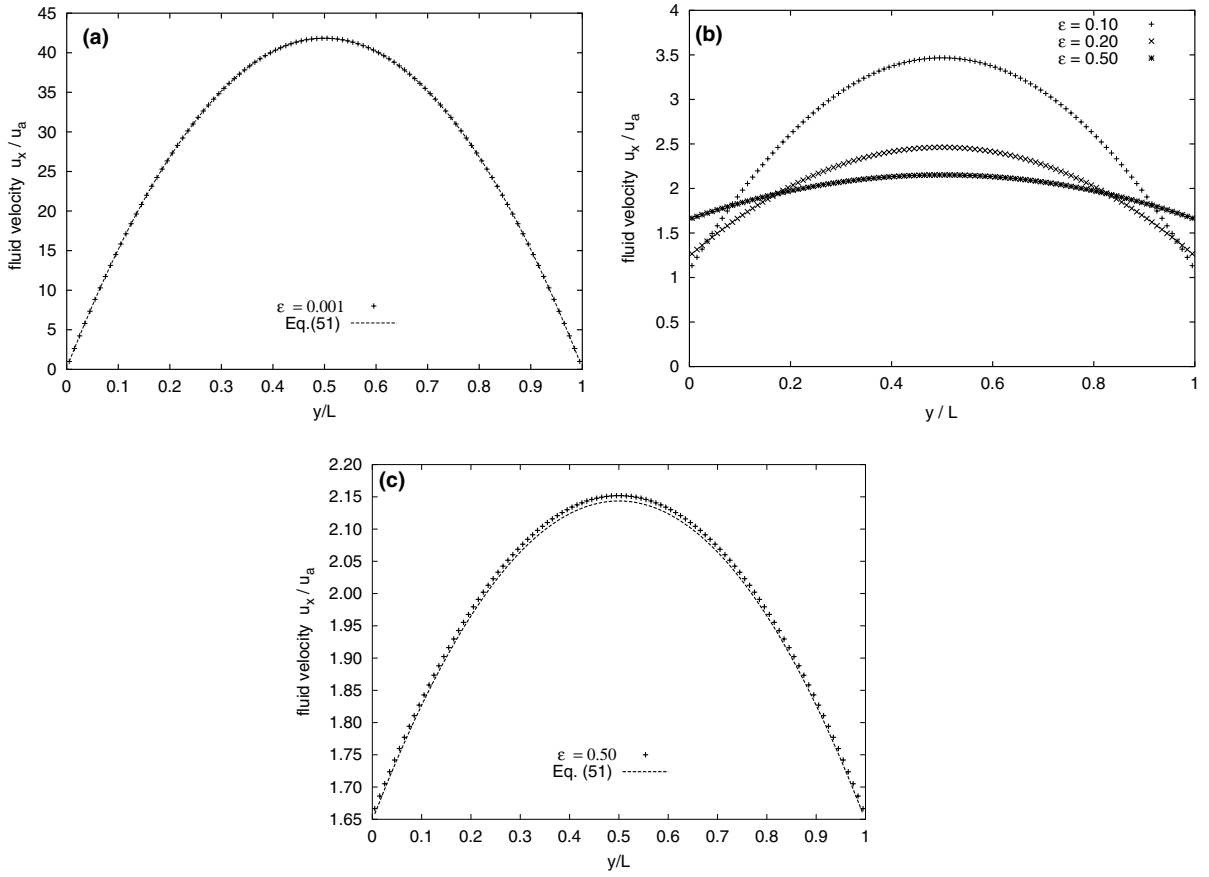

Fig. 9. Velocity profiles of Poiseuille flow for various values of the Knudsen number ε and $a = 0.001$ ($N_y = 100$ nodes).

tion scheme is used. These simulations were done with a constant value of the acceleration ($a = 0.001$) for $c = 1$, $L = 1$. We see that the slip velocity increases with the Knudsen number ε, while the parabolic velocity profile becomes more and more flattened, as observed by other authors [5,40]. Fitting this data shows that these velocity profiles are close to the analytical solution (51) where $C_1 = 1$ and $C_2 = 0.666$. Even for $\varepsilon = 0.50$, the largest difference between simulation results and the analytical solution (51) with the values of C_1 and C_2 mentioned above, is approximately 0.5% (Fig. 9c). In Fig. 10, we show the effect of the Knudsen number on the quantities $u_{\max}/\bar{u}$ and $u_{\text{slip}}/\bar{u}$. The agreement with Eqs. (54) and (55) with $C_1 = 1$ and $C_2 = 0.666$ is excellent, although we have no theory for this value of C_2.

Since the apparent value of the kinematic viscosity ν is dependent on the relaxation time τ and the lattice spacing δs [13], the value of the coefficient A given by Eq. (49) changes with the relaxation time τ, i.e., with the Knudsen number. To investigate the effect of the Knudsen number on the slip velocity in Poiseuille flow, we performed another set of computer simulations, where the acceleration a was always adjusted in order to keep a constant value of the reference quantity $u_\varepsilon = 0.001$ in the parabolic expression Eq. (59) of the fluid velocity profile. In this case (Fig. 11), we get a family of parabolic profiles whose shape is identical (all parabolae may be superposed after translation), while the slip velocity (the translation parameter) is dependent on the Knudsen number. For fixed Knudsen number and the same lattice spacing, the slip velocity is dependent on the boundary scheme (Fig. 12). To clarify this problem and to investigate also the effect of the

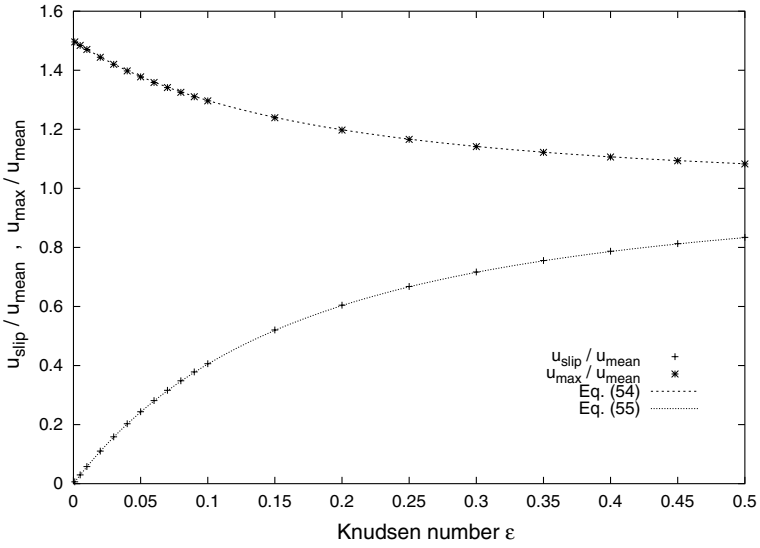

Fig. 10. Dependence of $u_{\max}/\bar{u}$ (upper curve) and $u_{\text{slip}}/\bar{u}$ (lower curve) on the Knudsen number for Poiseuille flow with the diffuse reflection boundary condition (version 1) and $a = 0.001$. Simulation results are marked × and +, respectively. The analytical results, Eqs. (54) and (55), are plotted with $C_1 = 1$ and $C_2 = 0.666$.

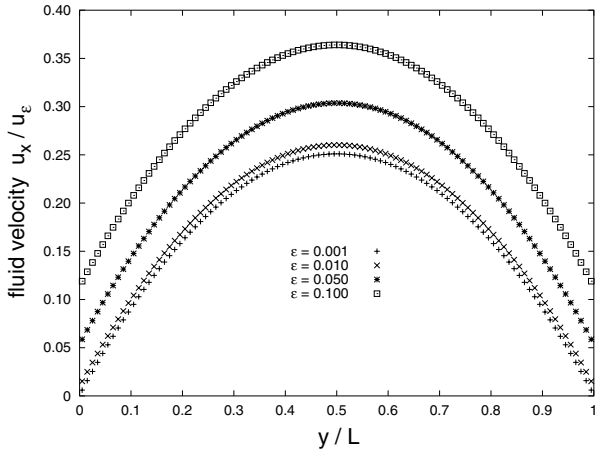

Fig. 11. Non-dimensional velocity profiles of Poiseuille flow ($N_y = 100$ nodes) for version 1 of the diffuse reflection boundary condition and various values of the Knudsen number.

lattice spacing and Knudsen number on the slip velocity, we performed a series of systematic computer runs using the bounce back, as well as the three versions of the diffuse reflection boundary conditions introduced in this paper. The results were compared with the following expression of the velocity profile, which is a generalisation of Eq. (59):

$$u_x(y) = u_\varepsilon[-(y/L)^2 + (y/L)] + u_{\text{slip}}, \tag{64}$$

where

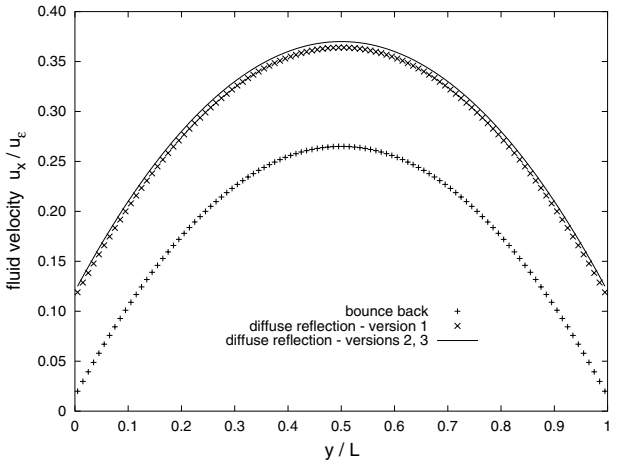

Fig. 12. Non-dimensional velocity profiles of Poiseuille flow (N_y = 100 nodes) for all boundary conditions discussed in this paper.

$$u_{\text{slip}}/u_\varepsilon = D_1\left(\frac{\delta s}{2L}\right) + D_2\left(\frac{\delta s}{2L}\right)^2 + C_1\varepsilon + 2C_2\varepsilon^2. \tag{65}$$

The form of Eq. (65) can be motivated by replacing Eqs. (50) with equations containing the fluid velocities at the appropriate nodes in Fig. 4 to which the LB boundary conditions actually relate. This is done in Appendix A and results in $D_1 = 0$ and $D_2 = 1$ for diffuse reflection version 1 and $D_1 = D_2 = 1$ for diffuse reflection versions 2 and 3. The vanishing value of the D_1 coefficient for the version 1 is an effect of the first-order interpolation procedure used to compute the values of the distribution functions in the ghost nodes.

Fig. 13 shows the effect of the Knudsen number on the slip velocity for constant lattice spacing ($\delta s = 0.01$) while Fig. 14a, b show the effect of the lattice spacing on the slip velocity for constant Knudsen number. Table 1 shows the values of the coefficients in Eq. (65), that match the graphical results in Figs. 13 and 14. Although the value $D_1 = 0$ is not a surprise for the bounce back scheme (in fact, this value matches other authors [3,41]), the vanishing value of the coefficient C_1 which is observed in the case of this scheme

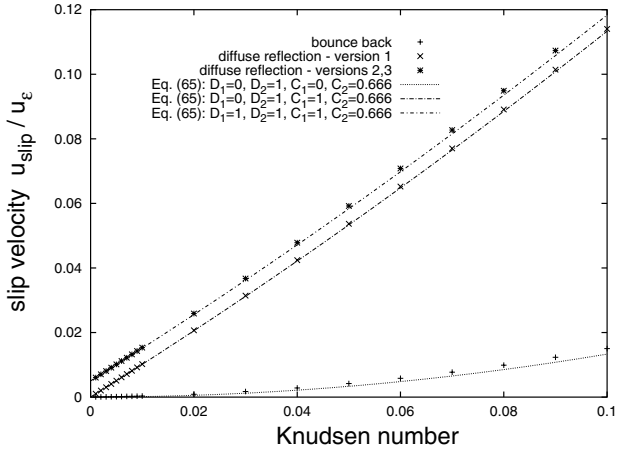

Fig. 13. Effect of the Knudsen number on the slip velocity in Poiseuille flow with $u_g/2v = 0.001$, for constant lattice spacing ($\delta s = 0.01$).

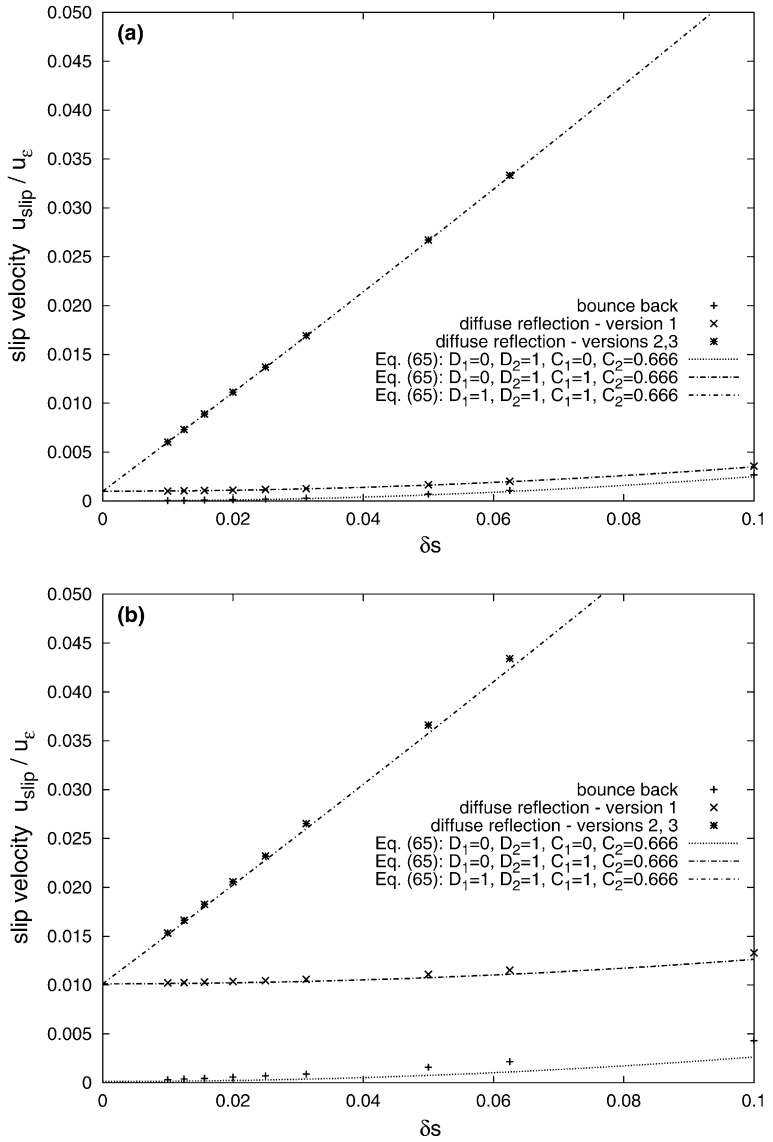

Fig. 14. Effect of the lattice spacing on the slip velocity in Poiseuille flow with $u_\varepsilon/2v = 0.001$, for two values of the Knudsen number: (a) $\varepsilon = 0.001$; (b) $\varepsilon = 0.010$.

Table 1
Values of the coefficients in Eq. (65) as suggested by LB simulation of Poiseuille flow using the boundary conditions introduced in this paper

	C_1	C_2	D_1	D_2
Bounce back	0	0.666	0	1
Diffuse reflection – version 1	1	0.666	0	1
Diffuse reflection – versions 2 and 3	1	0.666	1	1

does not agree with the widely accepted value $C_1 = 1$ derived in kinetic theory [5,29,32,37]. The values of the coefficients C_1 and C_2 are the same for all versions of the diffuse reflection boundary condition because of the kinetic mechanism involved in the diffuse reflection process.

7. Conclusions

In this paper, we introduced three procedures to handle the diffuse reflection boundary conditions in a two dimensional FDLB model. The model was subsequently used to simulate the stationary fluid flow between parallel plates. For both Couette and Poiseuille flow, we found evidence of fluid slip near the walls when using the three procedures for diffuse reflection boundary conditions. For Poiseuille flow, the slip velocity was also present when using the bounce back scheme widely used in the LB literature. Systematic investigations were done to study the effect of the Knudsen number as well as of the lattice spacing on the magnitude of the slip velocity in the stationary regime.

The slip velocity was found to be significant when the Knudsen number becomes larger than 0.01, as expected in accordance to kinetic theories. For constant lattice spacing, the slip velocity is expressed as a second-order polynomial in the Knudsen number ε. When using the diffuse reflection boundary condition, the coefficient C_1 of ε in this polynomial was found to be always equal to 1, a result which is in accordance to Maxwell's theory for an ideal gas. This coefficient is found to vanish when using the bounce back boundary condition to simulate the Poiseuille flow.

In the case of the Poiseuille flow, the bounce back and the version 1 of our procedure to handle the diffuse reflection boundary condition give a second-order dependence of the slip velocity with respect to the lattice spacing δs when the Knudsen number is constant. Versions 2 and 3 of the diffuse reflection procedure give both a first order and a second-order dependence on the lattice spacing. This can be related to the fact that for versions 2 and 3, the thermal mixing occurs in the ghost nodes. We conclude that version 1, in which the diffuse reflection occurs at a half lattice spacing outside the boundary nodes, gives the best results, a realistic dependence on Knudsen number and only a weak dependence on the lattice spacing. This is the main result of our systematic study and justifies the use of version 1 of the diffuse reflection boundary condition for further applications of FDLB models.

Implementation of the diffuse reflection boundary condition allows one to use LB models for the investigation of flow phenomena at the microscopic level, which are important for the development of micro-electro-mechanical-systems (MEMS).

Acknowledgments

This work was supported by the NASA OBPR Grant NNM04AA16G. V.S. acknowledges also the support of the Romanian Academy (Grant GAR 416/2003).

Appendix A

To clarify the values of the D coefficients for all versions of the diffuse reflection boundary condition, we recall that, for version 1 we have (in the stationary state)

$$\begin{aligned} u_x(0) &= \frac{1}{2}[u_x(\delta s/2) + u_x(-\delta s/2)], \\ u_x(L) &= \frac{1}{2}[u_x(L - \delta s/2) + u_x(L + \delta s/2)]. \end{aligned} \tag{A.1}$$

After introducing the above expressions in Eqs. (50) and solving for the coefficients B and C in (48), we get

$$B = -A,$$
$$C = -A\left[\left(\frac{\delta s}{2L}\right)^2 + C_1\varepsilon + 2C_2\varepsilon^2\right]. \tag{A.2}$$

For versions 2 and 3, Eqs. (50) are replaced by

$$u_x(-\delta s/2) = C_1\varepsilon B - 2C_2\varepsilon^2 A,$$
$$u_x(L + \delta s/2) = -C_1\varepsilon(2A + B) - 2C_2\varepsilon^2 A, \tag{A.3}$$

which give

$$B = -A,$$
$$C = -A\left[\left(\frac{\delta s}{2L}\right) + \left(\frac{\delta s}{2L}\right)^2 + C_1\varepsilon + 2C_2\varepsilon^2\right]. \tag{A.4}$$

In the stationary state, we should have $u_x(0) = u_x(L) = u_{\text{slip}}$ when using the bounce back boundary condition. From Eq. (A.1) we get, after using Eqs. (64) and (65),

$$u_x(0) = \frac{1}{2}[u(\delta s/2) + u(-\delta s/2)] = D_1\frac{\delta s}{2L} + (D_2 - 1)\left(\frac{\delta s}{2L}\right)^2 + C_1\varepsilon + 2C_2\varepsilon^2. \tag{A.5}$$

The relation above should be valid for arbitrary lattice spacing δs. This requires $D_1 = 0$ and $D_2 = 1$. The same result is recovered when using $u_x(L) = 0$ and (A.1).

References

[1] D.H. Rothman, S. Zaleski, Lattice Gas Cellular Automata: Simple Models of Complex Hydrodynamics, Cambridge University Press, Cambridge, 1997.
[2] B. Chopard, M. Droz, Cellular Automata Modeling of Physical Systems, Cambridge University Press, Cambridge, 1999.
[3] D.A. Wolf–Gladrow, Lattice Gas Cellular Automata and Lattice Boltzmann Models, Springer, Berlin, 2000.
[4] S. Succi, The Lattice Boltzmann Equation for Fluid Dynamics and beyond, Oxford University Press, Oxford, 2001.
[5] G.E. Karniadakis, A. Beskok, Micro Flows: Fundamentals and Simulation, Springer, New York, 2002.
[6] X. Nie, G.D. Doolen, S. Chen, Lattice Boltzmann simulations of fluid flows in MEMS, J. Statist. Phys. 107 (2002) 279–289.
[7] C.Y. Lim, C. Shu, X.D. Niu, Y.T. Chew, Application of lattice Boltzmann method to simulate microchannel flows, Phys. Fluids 14 (2002) 2299–2308.
[8] N. Cao, S. Chen, S. Jin, D. Martinez, Physical symmetry and lattice symmetry in the lattice Boltzmann method, Phys. Rev. E 55 (1997) R21–R24.
[9] R. Mei, W. Shyy, On the finite difference-based lattice Boltzmann method in curvilinear coordinates, J. Comput. Phys. 143 (1998) 426–448.
[10] T. Seta, K. Kono, D. Martinez, S. Chen, Lattice Boltzmann scheme for simulating two-phase flows, JSME Int. J. Ser. B 43 (2000) 305–313.
[11] T.H. Lee, C.L. Lin, A characteristic Galerkin method for discrete Boltzmann equation, J. Comput. Phys. 171 (2001) 336–356.
[12] W. Shi, W. Shyy, R. Mei, Finite-difference-based lattice Boltzmann method for inviscid compressible flows, Numer. Heat Transfer, Part B 40 (2001) 1–21.
[13] V. Sofonea, R.F. Sekerka, Viscosity of finite difference Lattice Boltzmann models, J. Comput. Phys. 184 (2003) 422–434.
[14] Y.H. Qian, D. D'Humières, P. Lallemand, Lattice BGK models for Navier–Stokes equation, Europhys. Lett. 17 (1992) 479–484.
[15] X. He, L.S. Luo, A priori derivation of the lattice Boltzmann equation, Phys. Rev. E 55 (1997) R6333–R6336.
[16] X. He, L.S. Luo, Theory of the lattice Boltzmann method: from the Boltzmann equation to the lattice Boltzmann equation, Phys. Rev. E 56 (1997) 6811–6817.
[17] L.S. Luo, Theory of the lattice Boltzmann method: Lattice Boltzmann models for nonideal gases, Phys. Rev. E 62 (2000) 4982–4996.

[18] M. Watari, M. Tsutahara, Two-dimensional thermal model of the finite-difference lattice Boltzmann method with high spatial isotropy, Phys. Rev. E 67 (2003) 036306.
[19] E.F. Toro, Riemann Solvers and Numerical Methods for Fluid Dynamics, second ed., Springer, Berlin, 1999.
[20] P. Bhatnagar, E.P. Gross, M. Krook, A model for collision processes in gases i: small amplitude processes in charged and neutral one-component systems, Phys. Rev. 94 (1954) 511–525.
[21] P. Welander, On the temperature jump in a rarefied gas, Ark. Fys. 7 (1954) 507–553.
[22] S. Chen, G.D. Doolen, Lattice Boltzmann method for fluid flows, Ann. Rev. Fluid Mech. 30 (1998) 329–364.
[23] N.S. Martys, X. Shan, H. Chen, Evaluation of the external force term in the discrete Boltzmann equation, Phys. Rev. E 58 (1998) 6855–6857.
[24] H. Grad, On the kinetic theory of rarefied gases, Commun. Pure Appl. Math. 2 (1949) 331–407.
[25] J.M. Burgers, Flow Equations for Composite Gases, Academic Press, New York, 1969.
[26] V. Sofonea, R.F. Sekerka, BGK models for diffusion in isothermal binary fluid systems, Physica A 299 (2001) 494–520.
[27] W.H. Press, S.A. Teukolsky, W.T. Vetterling, B.P. Flannery, Numerical Recipes in Fortran: the Art of Scientific Computing, Cambridge University Press, Cambridge, 1992.
[28] K.A. Hoffmann, S.T. Chiang, Computational Fluid Dynamics, third ed., Engineering Education System, Wichita, KS, 1998.
[29] W.G. Vincenti, Ch.H. Kruger, Introduction to Physical Gas Dynamics, Wiley, New York, 1965.
[30] C. Cercignani, Rarefied Gas Dynamics, from Basic Concepts to Actual Calculations, Cambridge University Press, Cambridge, 2000.
[31] Y. Sone, Theoretical and Numerical Analyses of the Boltzmann Equation – Theory and Analysis of Rarefied Gas Flows, Part I, Lecture Notes, Department of Aeronautics and Astronautics, Graduate School of Engineering, Kyoto University, 1998. Available from: <http://www.users.kudpc.kyoto-u.ac.jp/a50077>.
[32] M. Gad-el-Haq, The fluid mechanics of microdevices, J. Fluids Eng. – Trans. ASME 121 (1999) 5–33.
[33] K. Aoki, Dynamics of Rarefied Gas Flows: Asymptotic and Numerical Analyses of the Boltzmann Equation, Proc. of the 39th AIAA Aerospace Sciences Meeting & Exhibit, 8–11 January 2001, Reno, Nevada, American Institute of Aeronautics and Astronautics Meeting Paper AIAA 2001-0874.
[34] G. Mo, F. Rosenberger, Molecular dynamics simulations of flow with binary diffusion in a two-dimensional channel with atomically rough walls, Phys. Rev. A 44 (1991) 4978–4985.
[35] J. Koplik, J.R. Banavar, No slip condition for a mixture of two liquids, Phys. Rev. Lett. 80 (1998) 5125–5128.
[36] H. Brenner, V. Ganesan, Molecular wall effects: are conditions at a boundary ''boundary conditions''?, Phys. Rev. E 61 (2000) 6879–6897.
[37] R.W. Barber, D.R. Emerson, A numerical study of low Reynolds number slip flow in the hydrodynamic development region of circular and parallel plate ducts, Daresbury Laboratory Technical Report DL-TR-01-001, 2001.
[38] W. Marques Jr., G.M. Kremer, F.M. Sharipov, Couette flow with slip and jump boundary conditions, Continuum Mech. Thermodyn. 12 (2000) 379–386.
[39] J.C. Maxwell, On stresses in rarified gases arising from inequalities of temperature, Philos. Trans. Roy. Soc. London 170 (1879) 231–256.
[40] T. Inamuro, M. Yoshino, F. Ogino, A non-slip boundary condition for lattice Boltzmann simulations, Phys. Fluids 7 (1995) 2928–2930.
[41] R. Cornubert, D. d'Humières, D. Levermore, A Knudsen layer theory for lattice gases, Physica D 47 (1991) 241–259.